SSRG International Journal of Mechanical Engineering
ISSN: 2348-8360/ https://doi.org/10.14445/23488360/IJME-V11I5P107

Volume 11 Issue 5, 70-86, May 2024

Original Article

Towards Digital Twin and Augmented Reality Modelling to Mitigate Silica Scaling in Geothermal Plants

Admire Chityori[1*], Jean Bosco Byiringiro[2], Rehema Ndeda[1,3], Benson Gathitu[4]

[1]*Department of Mechatronic Engineering, Pan African University for Basic Sciences, Technology and Innovation, Kenya.*
[2]*Siemens Mechatronics Certification Centre, Dedan Kimathi University of Technology, Kenya.*
[3]*Department of Mechatronic Engineering, Jomo Kenyatta University of Agriculture and Technology, Kenya.*
[4]*Department of Agricultural and Biosystems Engineering, Jomo Kenyatta University of Agriculture and Technology, Kenya.*

[1]*Corresponding Author : chityori.admire@gmail.com*

Received: 11 March 2024 Revised: 15 April 2024 Accepted: 13 May 2024 Published: 31 May 2024

Abstract *- Silica scaling in geothermal reinjection reduces efficiency, increases costs, and causes downtime. An elevated concentration of silica is experienced in the separator tank after depressurizing the brine. This causes amorphous silica to exceed its solubility limit, causing supersaturation, clogging and disrupting steam production. The study investigated the use of digital twins, augmented reality, and Industrial Internet of Things technologies for remote real-time monitoring and control of silica treatment. A laboratory-synthesized geothermal fluid with an initial concentration of 90 mg/L was prepared. Silica concentration was determined using the molybdate method with an MRC UV/VIS16-spectrophotometer. A response surface methodology based on Box Behnken was used to develop a model for optimal conditions of silica precipitation. Analytic Process Control System (APCS) system using PLC was used to monitor and control synthetic geofluid pH, volume and temperature while silica precipitation was observed. 0.9M of NaOH was introduced to geofluid to maintain a setpoint, pH11. The AR-DT model was used for real-time remote monitoring and control to avert silica scale buildup at pH11. Maximum silica extraction of 96.38% was observed at pH7.5, temperature of 80°C, volume of 5.5 L and lowest silica extraction of 66.90% was observed at pH5.5, temperature of 50°C and volume of 5.5L. The DT and AR model effectively simulated geofluid behaviour, communicating with APCS using IIoT via MQTT protocol, enabling real-time data exchange. Deviations in pH from setpoint triggered corrective action based on using historical and real-time data, sending a signal to the PLC to adjust the NaOH solution dosage. The AR model provided an immersive experience, enhancing monitoring and control efficiency.*

Keywords *- Augmented reality, Box behnken, Digital twin, Industrial Internet of Things, Silica scaling.*

1. Introduction

Geothermal energy is a renewable and environmentally friendly energy source that efficiently harnesses heat stored in geothermal reservoirs, often in the form of hot water or steam [1]. This energy is used to drive turbines, thereby generating electrical power. Geothermal energy has several notable benefits, including its inherent sustainability, consistent reliability, and minimum carbon emissions [2, 3].

One of the key challenges that arise during the utilisation of geothermal energy is silica scaling and corrosion. The Earth's crust and mantle are primarily composed of oxygen and silicon, which combine to create the intricately correlated silicate species SiO_4^{4-} [4]. The operational factors, such as temperature, pressure, pH, flow rate and volume, have a major effect on the occurrence of silica scaling in geothermal plants by affecting supersaturation levels and kinetics of polymerisation [5]. During steam extraction processes, the depressurization of geothermal fluid lowers the fluid temperature range to 100 °C - 130 °C. At this temperature, the fluid's capacity to retain dissolved silica is restricted, resulting in supersaturation [6, 7]. Oversaturated in the geothermal fluid causes the silica to solidify as amorphous silica and create a silica scale through the process of polymerisation of monomeric silica [8]. This happens when the Silica Saturation Index (SSI) ultimately reaches or surpasses SSI ≥ 1. These deposits not only reduce operational efficiency but also pose a risk to the equipment.

During reinjection, scale buildup within the reinjection pipes causes blockage, leading to a decrease in the amount of brine being reinjected. This may necessitate well reaming or drilling a new well, which is capital intensive. Implementing scaling prevention measures in the subsurface pipelines, reinjection, and overlying formation is, therefore, necessary to effectively mitigate the occurrence of amorphous silica scale [9].

Several methods, such as high-temperature reinjection, cationic polymer precipitants and pH modification

procedures, have been widely adopted worldwide to reduce silica deposition [8, 10]. The high-temperature reinjection method involves the reinsertion of geothermal brine, which has been cooled throughout the power-generating process, into the underground reservoir at elevated temperatures. A drawback of the high-temperature reinjection technique is the inefficient utilisation of energy, as the brine is unable to completely extract the thermal energy before being reinjected into the reservoir. The pH correction procedure involves acidifying the geothermal brine by adding hydrochloric acid or sulfuric acid until its pH drops below 6 [11]. Furthermore, the process of reducing the pH level to less than 6 gives rise to uncertainties regarding the possible corrosion of pipelines and the creation of anhydrite in the geothermal reservoir [8, 12].

The seed-induced precipitation process is thought to be the most promising. These seeds possess a strong attraction to blend with silicic acid in the geothermal brine. The potential of amorphous silica seeds to stimulate the nucleation and polymerisation of silicic acid has been studied and used in some geothermal power plants [13]. By introducing these seeds, the precipitation process is accelerated, hence decreasing the probability of silica deposition on the surfaces of the pipeline.

Researchers have also adopted the practice of injecting silica seeds, silica gel, as well as Mg^{2+}, Ca^{2+} and Al^{3+} ions into the brine to remove excess silica and avoid the formation of silica deposits [6, 8, 13]. The rate of silica precipitation is enhanced by the presence of ions such as Mg^{2+} and Ca^{2+} when sodium hydroxide or calcium hydroxide is added. These ions react with silica to generate Magnesium-Silicate-Hydroxide (M-S-H) or Calcium-Silicate-Hydroxide (C-S-H) phases. The C-S-H and M-S-H phases become oversaturated at alkaline pH (i.e. pH>8.5), leading to their precipitation because $H_3SiO_4^-$ species promote the adsorption of ions with a valence of two on the surface [6, 14].

The addition of NaOH to pH 10 resulted in an 80% reduction in silica, with a ratio of 200 ppm silica/200 ppm Mg^{2+} [4]. Nevertheless, the reaction durations required for the removal of silica are not conducive to continuous operation in a geothermal plant. Hence, it would be advantageous to optimise the reaction time. Putera et al**.** [15] employed a full factorial design to achieve the highest reduction in silica at a pH of 9, a temperature of 70 °C, and a reaction period of 5 minutes. The study undertaken was limited by the unknown concentration of calcium hydroxide, which prevented the determination of the optimal parameters for achieving optimal silica reduction. Hence, it is crucial to use a known concentration of calcium hydroxide to ensure optimal conditions for the Si-reduction procedure.

Despite these current approaches, silica scaling remains a major challenge in the operation of geothermal power plants. The main reason is that silica scaling is not always homogenously distributed, so it may be hard to clean or remove all the scaling [16]. Conventional methods for monitoring and controlling silica scaling are currently employed, such as manual inspection and maintenance, which are labour intensive and susceptible to human fallibility. The existing solutions lack the capability for remote monitoring and control. They cannot also offer real-time information and visualisation regarding equipment status and the scaling process, hence impeding the prompt detection of system alterations and the subsequent implementation of necessary measures.

At present, a few technologies have been implemented to control or monitor silica scaling remotely in geothermal plants. Taddei et al. [17] developed a retention system technology to control and reduce silica scale formation before reinjection. The retention system design aimed at controlling and reducing the rates at which silica scale deposits form by taking into account factors such as pH, temperature, and brine composition. The system enhances the process of polymerisation inside the tank, hence preventing the formation of scale deposits in the pipes of the reinjection well. Silica concentration reduction dropped from 451 ppm to 265 ppm. However, the limitation of this method is that excessive salt levels might impede the effective implementation of a silica polymerisation ageing technique due to the potential formation of silica deposits.

The utilisation of fibre optics, electrolysis, and electrocoagulation has garnered more interest in the ongoing efforts to address the silica scaling issue in a more technologically advanced manner. The electrocoagulation technique employs iron electrodes to generate a floc that quickly settles when left undisturbed, thus enabling the elimination of silica from the fluid. Mroczek et al. [18] employed an electrocoagulation method which effectively eliminated silica, resulting in a quick decrease in silica concentration. Experimental parameters were electrode material, pH, temperature, current and circulation flow rate. The laboratory investigations showed that iron electrodes were effective in lowering silica concentrations in ageing geothermal water as silica concentration rapidly dropped from 600 mg/L to 100 mg/L.

Yoshihiko et al. [19] successful removal of silica was achieved through the reaction with hydroxide ions produced via water electrolysis. By increasing the electrical current in the reaction solution, the formation of calcium carbonate is facilitated, hence assisting in the segregation of silica and calcium from the solution.

A small quantity of silica remained after subjecting it to a current of 5 A, while a greater amount of silica remained after subjecting it to a current of 3 A, both at a flow rate of 50 mL/min. However, the production of precipitates might be hindered by large currents caused by the migration of protons

from the anode to the cathode phases. Also, there is a need for further investigation to determine the optimal parametric conditions for achieving maximal silica removal.

Fibre optics for real-time monitoring was studied by Okazaki et al. [20]. An exposed core length fibre optic sensor was immersed in geothermal water containing 980 mg/L dissolved silica at 93 °C. The sensor operates by monitoring the decrease of transmittance due to the presence of scales on its surface. The transmittance responses were tested throughout a wavelength range of 500 to 1700 nm, using an exposed core length of 24 cm. The sensor successfully quantified the impact of pH variations on the production of silica scale within a time frame of 6 hours, therefore showcasing its potential to detect real-time changes promptly. Though this method has high sensitivity, allowing for real-time remote monitoring, it is limited to the detection of silica deposits.

The increase in technological applications for industrial process monitoring and control offers the potential to improve efficiency, reduce costs, and increase safety in industrial operations. Tao et al. [21] define a digital twin as a combination of three elements: the physical product, the virtual product, and the connected data that links the physical and virtual aspects. It is distinguished by its capacity to replicate, imitate, or oversee the system or physical surroundings [22]. On the other hand, Augmented Reality (AR) refers to a collection of technologies that enhance the perspective of the real-world environment by adding computer-generated components or objects [23].

The integration of digital twins and augmented reality is being used in diverse industrial processes. Caiza and Sanz [24] presented a DT and AR for smart manufacturing. The methodology entails acquiring data on physical processes, constructing a virtual environment, and transmitting information about the physical setting. The system facilitates bi-directional communication between the physical and virtual environment, visualized using AR. Alexios and Panagiotis [25] employ a DT as a dynamic model to continuously observe and adjust a laser-based manufacturing process while also developing a controller for the process. The DT successfully adjusted to the actual process by closely monitoring and managing intricate process dynamics.

Qiu et al. [26] highlighted the use of DT and AR technologies for industries operating under Industrial Internet of Things (IIoT) architecture for more accurate and timely data collection and analysis, thereby allowing more effective maintenance and repair processes. Hasan et al. [27] enhanced building processes by implementing a combination of DT, AR, and physical system integration. The DT server operates as a virtual replica, acquiring and retaining current data and information regarding the machinery. An application utilising AR was used to overlay virtual information onto the actual model, providing users with a visual and interactive experience.

Geothermal operations have successfully implemented Digital Twin technology. A modelling framework called GOOML has been developed for creating digital twins of geothermal power plants based on hybrid data-driven thermodynamics component-based systems models [28]. This framework has been extensively utilised in various geothermal power plants, yielding highly accurate outcomes. The GOOML, developed by Buster et al. [29], effectively simulates the real-world performance attributes of geothermal systems. The model has two frameworks: a historical system and a prediction system.

The geothermal system's measured parameters were pressure, temperature, and mass flow in order to determine the thermodynamic characteristics of the working fluid precisely. This was essential for assuring the effective operation and optimisation of geothermal power plants. Taverna et al. [30] GOOML framework has been used to create digital twins that offer steam field operators operational environments for analysing and comprehending historical and predicted power generation, investigating new steam field possibilities, and pursuing optimal asset management in real-world applications.

Thus, there is potential for the utilisation of a DT server in geothermal plants for real-time monitoring of the silica extraction process. Additionally, the AR technology provides users with a visual and interactive platform of the plant processes. The implementation of AR, DT, and IIoT technologies into industrial systems has shown considerable potential in enhancing plant efficiency and reducing maintenance expenses. Therefore, the successful use of these technologies in maintenance across several sectors emphasises their potential as a groundbreaking technology. The capacity to overlay real-time data onto the actual environment, allowing for remote monitoring and enhanced training and safety requirements, has proven very advantageous in the many situations that have been covered.

Given these accomplishments, it is feasible to anticipate that using AR and DT for monitoring geothermal chemical processes in this study might provide significant benefits. Thus, adopting AR and DT technologies in geothermal chemical plants can potentially enhance the clarity and comprehension of plant operations. It can also improve operational effectiveness by monitoring and controlling silica deposition through the regulation of pH, temperature, and volume, which directly impact the process. It is necessary to examine the effectiveness of AR and DT in monitoring the accumulation of silica in geothermal power plants.

However, the current monitoring and control systems for silica scaling are limited, and it is difficult to detect and

mitigate the problem in real-time and remotely. Moreover, a significant number of these systems exhibit insufficient integration with control systems, impeding the automatic adjustment of operational parameters or the adoption of mitigation strategies in response to scaling problems.

Furthermore, several systems are tailored for certain applications or equipment, which implies that they could lack the essential flexibility and scalability needed to handle different operating circumstances or scaling scenarios. Several current systems rely on periodic analysis and cannot monitor in real-time. The combination of these limits poses significant barriers to effectively controlling silica scaling.

Therefore, it is necessary to investigate other methods that may reduce the silica concentration in the geofluid in order to mitigate silica scaling. Moreover, it is necessary to analyse several techniques that can monitor and control the treatment of silica scaling in remote and real-time. A fully automated simulation system capable of replication is needed to carry out experimental research on silica treatment in geothermal power plants. This system aims to improve or upgrade the current testing methods of the physical system without the need for conducting real tests on the physical plant, therefore enhancing its maintenance.

2. Materials and Methods

2.1. Experimental Study

A preliminary experiment was carried out to obtain optimal conditions for silica extraction which include NaOH concentration, brine pH, brine temperature, reaction and settling time and agitation speed. The experimental setup for the preliminary experiment is depicted in Figures 1(a), (b), and (c).

A geothermal fluid sample was created utilising synthetic ingredients, including sodium metasilicate and sodium chloride, with a precise concentration of 200 mg/L as described in [4]. Magnesium and calcium were introduced, mirroring the prevalent ions often present in natural geothermal brine [12]. The geothermal brine solutions were heated to different temperatures using the Intelligent Heating Oil Bath shown in Figure 1(a).

Different amounts of NaOH were then added to raise the pH of the brine to 11, while silica precipitation was observed, as depicted in Figure 1(b). After reaching setpoint pH, the geothermal fluid was allowed to settle, and the formation of silica precipitation was observed, as depicted in Figure 1(c).

Table 1 depicts the temperatures, NaOH concentrations and agitation speeds used in the preliminary study. The reaction time for each sample was recorded. The objective was to determine the concentration of NaOH, which gave maximum silica extraction in a shorter reaction time and was used for further experiments using the APCS machine.

The Amatrol Analytic Process Control system (APCS) T5554 was used to represent a typical geothermal plant. In our previous work, used the same machine for process modelling using virtual reality. The APCS comprises a Programmable Logic Control (PLC), metering pump, eductor pump, continuous stirred tank reactor, pH transmitter, two reagent tanks, and a pipe bypass network. The reactor tank on the APCS machine corresponds to the collection tank in the geothermal plant, shown in Figure 2(a).

The collection tank accumulates geothermal fluid from the separator tank and condensed water from the cooling water pool before transferring the fluid for reinjection. The reactor tank served as the treatment station prior to the fluid's reinjection. The APCS depicted in Figure 2(b) was used to control the pH, temperature and volume of the fluid using the optimised parameters obtained in the preliminary experiment. A coupled model for the geothermal industry was considered by not used due to the limitations of testing in the laboratory.

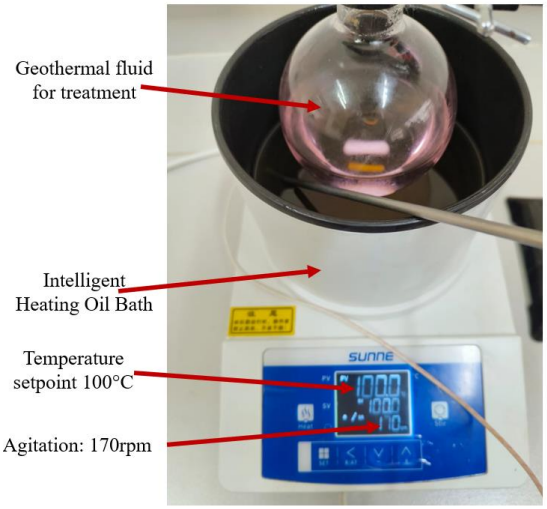

(a)

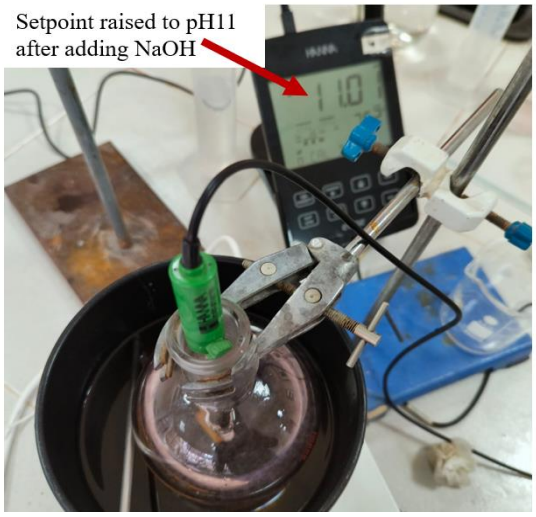

(b)

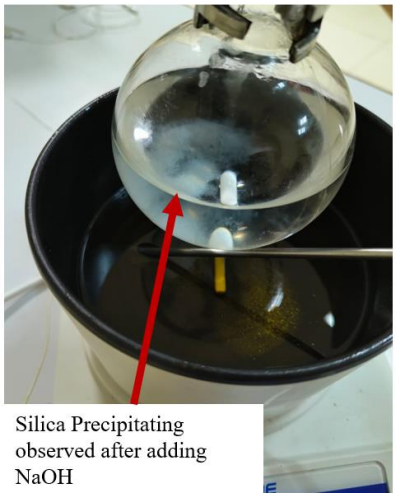

(c)

Fig. 1 Preliminary experiment setup (a) Intelligent Heating Oil bath heating the brine to a specified working temperature, (b) Dosing of the brine using NaOH to a setpoint pH 11, and (c) Silica precipitation observed after dosing with NaOH.

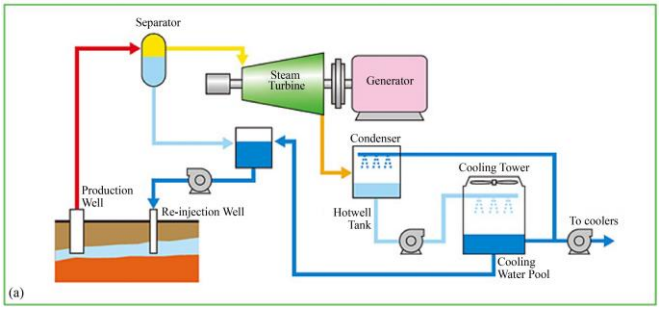

(a)

Fig. 2(a) Schematic layout and working principle of geothermal power plant (Source: https://global.kawasaki.com/en/energy/equipment/steam_turbines/geothermal_power.html), and (b) Analytic Process Control System

The silica extraction process was optimized using a three-factor, three-level Box-Behnken Design (BBD) with three repeated runs at the centre point based on the preliminary findings as specified in Table 2. Fifteen runs were executed using Minitab software (version 2021) and subsequently conducted according to the sequence specified in Table 3.

Table 1. Parameters used in the preliminary study

Temperature (°C)	NaOH Concentration (M)	Agitation speed (rpm)
115	0.3	170
	0.6	
	0.9	
	1.2	
	1.5	
100	0.3	200
	0.6	
	0.9	
	1.2	
	1.5	
80	0.3	230
	0.6	
	0.9	
	1.2	
	1.5	
60	0.3	260
	0.6	
	0.9	
	1.2	
	1.5	
40	0.3	300
	0.6	
	0.9	
	1.2	
	1.5	

The preparation of synthetic geofluid is represented in Figure 3.

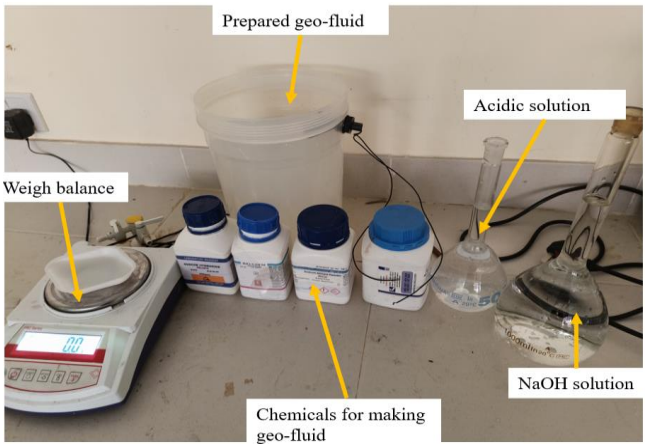

Fig. 3 Preparation of geothermal fluid and dosing chemical solutions

Table 2. Range and levels of parameters in Box-Behnken experimental design

Level				
Factor	**Symbol**	**Low**	**Middle**	**High**
Brine pH	A	5.5	6.5	7.5
Temperature	B	50	65	80
Volume	C	4.5	5.5	6.5

Table 3. Box Behnken design of experiments

Sample Runs	Brine pH	Temperature (°C)	Volume (L)
1	5.5	65	4.5
2	6.5	65	5.5
3	7.5	80	5.5
4	7.5	50	5.5
5	5.5	80	5.5
6	6.5	65	5.5
7	6.5	80	4.5
8	5.5	50	5.5
9	6.5	50	4.5
10	7.5	65	6.5
11	5.5	65	6.5
12	6.5	65	5.5
13	6.5	80	6.5
14	6.5	50	6.5
15	7.5	65	4.5

The DT and S7 1214 PLC were used for proactive monitoring and control of silica formation data. The APCS used a PID controller to manage the rate at which the basic solution (NaOH) was introduced. The peristaltic pump was used to provide a base solution into the reactor tank in order to attain and sustain a setpoint pH 11. The experimental setup is shown in Figure 4.

The agitation speed for fluid mixing was set at 200 rpm to prevent turbulence resulting from excessive mixing speeds. Excessive mixing rates lead to turbulent mixing, which is undesirable since it causes inaccuracies in pH readings. The treated solution was transferred to a settling tank and subsequently subjected to filtration using Whatman grade 41. The sludge was extracted for further processing, while samples of the supernatant were taken for silica concentration analysis. The response time and percentage silica extraction were quantified as response 1 and response 2 respectively. The acquired data was analysed using regression model analysis to establish the relationship between the responses and the independent variables.

To determine the absorbance of the silica, the molybdosilicate spectrophotometric method (ISO 2598-2:1992) was used [31, 32]. Various quantities of silica standard, ranging from 5 to 25 ppm (or mg/L), were prepared using a stock solution of silica. For each silica standard fluid sample, 50 ml of each was added to a 100 ml flask. Hydrochloric acid was diluted with water at a ratio of 1:1, and 1 ml of hydrochloric acid solution was added along with 2 ml of ammonium molybdate solution to the 50 ml silica standard sample solution. The samples were left undisturbed for 5 minutes, after which 2 ml of oxalic acid was introduced and thoroughly blended with each sample solution. Using a UV-Vis-16 spectrophotometer, the UV-VIS absorbance of the solution was measured at a wavelength of 420 nm to estimate the content of silicate. Figure 5 is a plot of the calibration curve for the absorbance for silica standards. The calibration curve was then used to determine the silica concentration that remained in the geothermal fluid after treatment.

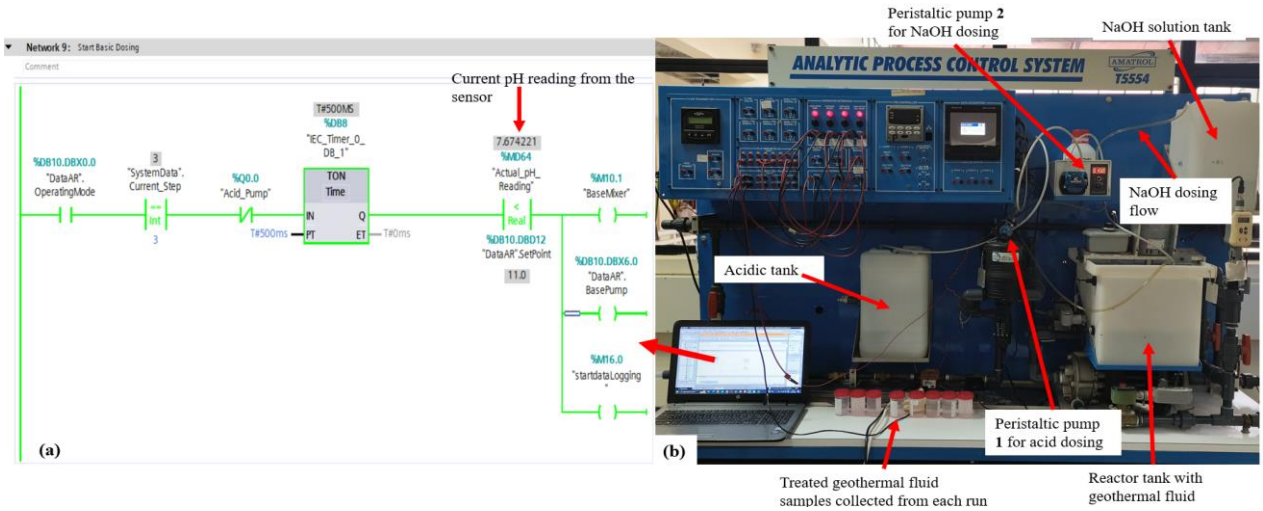

Fig. 4(a) PLC program to control the APCS, and (b) APCS experimental setup for geofluid treatment.

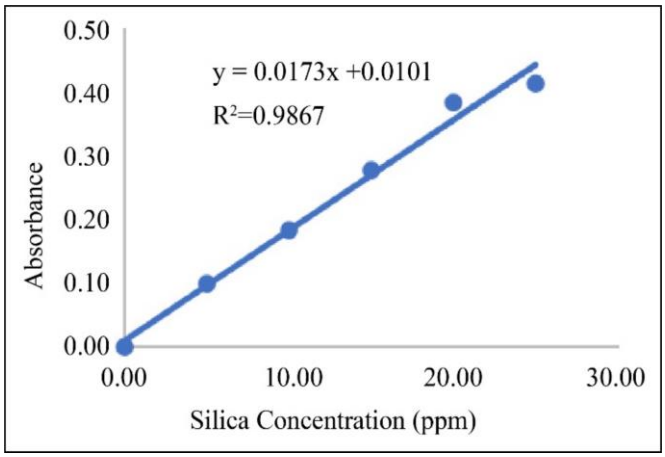

Fig. 5 Calibration of silica standards using UV/VIS-spectrophotometer

2.2. Digital Twin and Augmented Reality Model Development

The 3D CAD model of APCS was designed using Siemens NX and Blender software. The 3D CAD model was imported into Unity software (version 2022) for physics assignment and visual development of the components, as depicted in Figure 6. This intends to replicate the behavioural characteristics of the constituents in the physical environment. The 3D design took into account the dimensions, surfaces and materials of the APCS in order to produce the digital model. The ISO 16792 standard was used to enhance the 3D model by incorporating Product Manufacturing Information (PMI) [33]. The Unity3D and Vuforia Engine were used to develop an AR immersive virtual mobile application.

The process parameters, temperature, volume, and pH trends were written to align with the APCS machine operations. The physics assignments were completed via C# scripts and physical assets in Unity 3D. The inclusion of physics is crucial in this context since it facilitates the development of a digital replica of the APCS as the digital twin. In the C# scripts, the MQTT.net package was used to establish bi-directional communication between the DT-AR model and its physical counterpart. Figure 6 depicts the DT-AR model in Unity.

While implementing virtual commissioning and digital twin using Unity software, the first step was replicating the PLC controller. This was achieved by establishing a control logic operation for the APCS. The control logic of the machine was implemented using ladder logic and functions within the TIA software.

In the second phase, a bi-directional communication protocol was implemented to facilitate the flow of data and information between the physical machine and the DT-AR model. The PLC and IOT2040 served as gateways to enable the implementation of the Industrial Internet of Things (IIoT), enabling seamless communication over ProfiNET. Modelling and scripting were essential in the Unity programme to replicate the functionality of sensors, actuators, fluid behaviour, and the overall behaviour of the system linked to the controller. The dynamic reaction of the sensors and actuators was used to represent the response of the system correctly.

The third phase included the creation of the visualisation interface model. To enhance user engagement and enable monitoring of process parameters in the immersive environment, a User Interface (UI) panel and a graphing output displaying the pH trends were developed. Furthermore, it enabled the user to autonomously control the augmented reality system without relying on any external factors. The AR application was installed into a mobile phone through the Unity software.

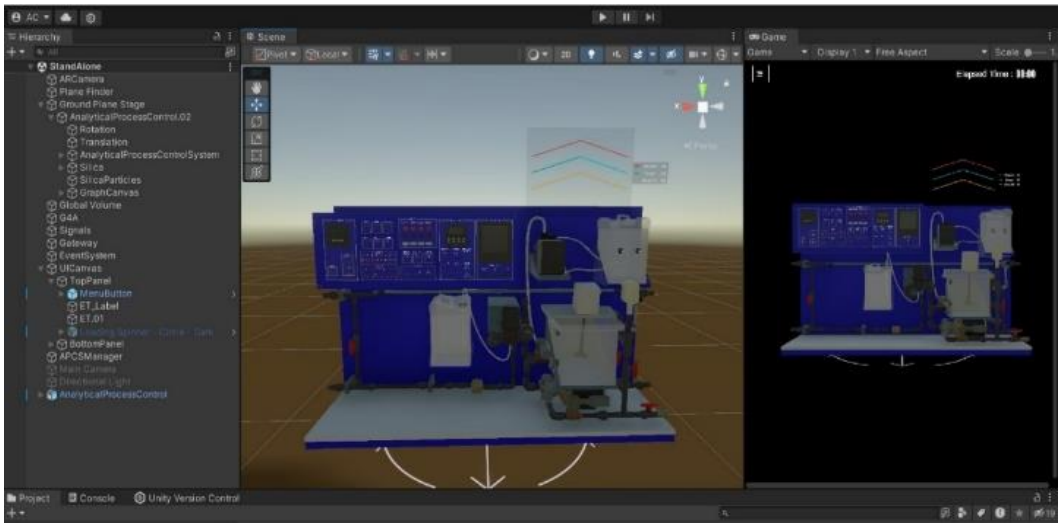

Fig. 6 APCS DT-AR model of development in Unity 3D

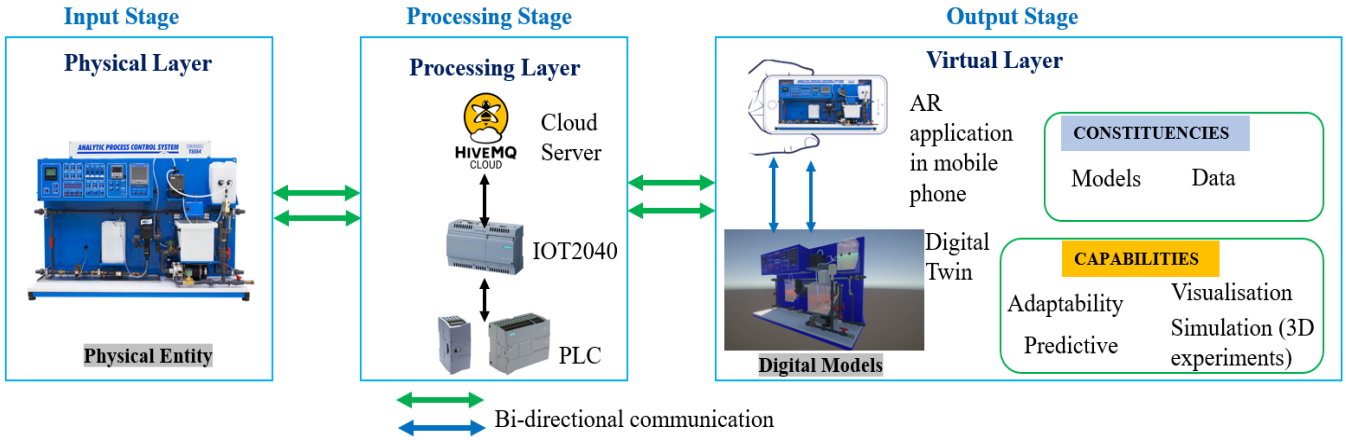

Fig. 7 Process flow and communication between the physical machine and the digital model

The fourth step was to ensure data transfer between the AR application and the APCS. The HiveMQ (MQTT broker) was used to enable data transfer and communication between an AR application and APCS. Message Queuing Telemetry Transport (MQTT) was used to provide bi-directional communication using TCP protocol. The C# scripts were developed in Unity using the MQTT.net package to establish communication with a PLC using an MQTT broker.

The APCS's data was sent to the virtual environment, and the virtual environment's instructions and commands were sent to the physical station. Each button that interacted with one of the variables from the PLC device contained all the necessary data for communication. The PLC tags were directly mapped into Unity using C# scripts and the Node-red feature in the IOT2040 module. This step closed the communication gap between the digital twin and its physical counterpart, as illustrated in Figure 7. The APCS machine was now controlled in real time.

The analytic machine was able to achieve real-time control via the seamless integration of physical and virtual systems. Consequently, altering the command signal immediately affected the performance and behaviour of the inputs or outputs. Data from the PLC was collected utilising the data log function of the PLC S7 1214 and then published on the internet. The process parameters were continually logged at a frequency of 1 Hz.

3. Results and Discussion

3.1. Analysis of Silica Extraction

The preliminary experiment determined that the optimal conditions for silica removal were when NaOH was added at a concentration of 0.9 M. The main emphasis, therefore, was on the efficacy of silica removal by adding NaOH at this optimal condition. By implementing a UV/Vis-16 spectrophotometer, the geothermal fluid exhibited an initial absorbance reading of 1.581, indicating a silica content of 90.803 ppm. Upon the addition of NaOH, the pH rapidly increased from the early pH values (5.5, 6.5, and 7.5) to the desired pH of 11, causing silica to precipitate. The equation from the calibration curve in Figure 5 was utilised to determine the new silica concentrations, and subsequently, the percentage of silica extracted was computed. The results are presented in Table 4.

Run 3 yielded the maximum percentage of silica extracted at a reaction time of 48 seconds, 80 ºC temperature and pH 7.5. Conversely, run 8 resulted in the lowest percentage of silica extracted, with 78 s reaction time, 50 ºC temperature and pH 5.5. Raising the pH to 11 led to a higher quantity of silica being formed as a precipitate, resulting in a lower concentration of silica in the fluid. This suggests a positive outcome. Runs 2, 4, 10, and 15 resulted in a silica extraction percentage of over 90 % and a shortened reaction time. The faster reaction occurs due to the alkaline nature of geothermal fluid at pH 7.5, which has a lower percentage of silica. When similarly alkaline NaOH is added, the reaction speeds up.

This finding is consistent with the results obtained by Putera et al. [15], who observed an increase in the rate of silica precipitation with an increase in pH. Their results showed that pH has more significance while temperature has less significance to the percentage of silica removed.

This can be attributed to the inert and mildly acidic properties of silica, which, when subjected to high temperatures and treated with a NaOH solution, yield favourable outcomes [34].

Using the data in Table 4, regression models were developed to establish the relationship between the responses. (reaction time and percentage of silica extracted) and the independent variables (pH, temperature and volume). This relationship is represented by two second-order polynomial equations, reaction time response, R1 (Equation 1) and silica extracted response, R2 (Equation 2).

Table 4. Box-Behnken experimental design and experiment responses

Factor Levels				Responses	
Sample Runs	**Brine pH**	**Temperature (°C)**	**Volume (L)**	**Reaction Time (s)**	**% of Silica Extracted**
1	5.5	65	4.5	75	82.37
2	6.5	65	5.5	64	91.45
3	7.5	80	5.5	48	96.38
4	7.5	50	5.5	56	91.60
5	5.5	80	5.5	71	80.97
6	6.5	65	5.5	63	86.07
7	6.5	80	4.5	55	89.88
8	5.5	50	5.5	78	66.90
9	6.5	50	4.5	67	86.00
10	7.5	65	6.5	55	92.05
11	5.5	65	6.5	73	79.57
12	6.5	65	5.5	60	86.77
13	6.5	80	6.5	59	89.38
14	6.5	50	6.5	70	78.36
15	7.5	65	4.5	52	93.70

$$R_1 = 244.5 - 29A - 0.276B - 13.3C + 0.96A^2 - 0.00019B^2 + 0.46C^2 - 0.0167AB + 1.25AC + 0.0167BC \quad (1)$$

$$R_2 = -89 + 36.7A + 2.12B - 15.4C - 1.56A^2 - 0.01145B^2 + 0.38C^2 - 0.155AB + 0.29AC + 0.119BC \quad (2)$$

Where A is brine pH, B is brine temperature, and C is brine volume.

To analyse the performance of the predictions in Equations 1 and 2, ANOVA is summarized in Table 5.

Table 5. Analysis of variance results for the models (Reaction time and Percentage of Silica Extraction)

Source of Variation	Response 1		Response 2	
	P-Value	**F-Value**	**P-Value**	**F-Value**
Model	0.001	26.95	0.019	7.62
pH	0.000	199.53	0.001	47.31
Temp	0.002	38.96	0.015	13.19
Volume	0.246	1.73	0.233	1.84
pH*pH	0.431	0.73	0.404	0.83
Temp *Temp	0.972	0.00	0.192	2.27
Volume *Volume	0.699	0.17	0.831	0.05
pH*Temp	0.826	0.05	0.217	2.00
pH*Volume	0.298	1.35	0.868	0.03
Temp*Volume	0.826	0.05	0.327	1.18

When examining ANOVA findings, a higher F-value coupled with a smaller p-value (i.e., $p<0.05$) indicates that the model is statistically significant. The p-values are less than 0.05 for both models; the reaction time and % of silica extraction imply that the variables play a significant role in the responses. P-values greater than 0.05 indicate that the variables are not significant to the models. The F values of 26.95 and 7.62 indicated a substantial model fit, which yielded a low p-value ($p<0.05$), indicating the model's strong significance for both responses (R1 and R2).

In addition, the high coefficients of determination (R-sq.) of 97.98 % and 93.2 % for reaction time and percentage of silica extraction, respectively, in Table 6, demonstrate a significant relationship between the measured and projected responses. These values fall within the permissible range (R>80 %) because it indicate a strong linear relationship of the variables and that the model explains a large portion of the variance in the data, which suggests that the model fits the data well.

The R-value near 100 % signifies that the model possesses a high degree of accuracy in predicting the response variable for future observations. In comparison, the R-value near 0 % indicates that the model is not proficient in predicting future responses.

Table 6. Models fitting results

Model Term	Full Quadratic Models	
	R1 Response	R2 Response
R-sq.	97.98	93.21
R-sq. (adj)	94.34	93.21
R-sq. (pred)	78.07	93.21

Table 7. Modified model fittings for optimised empirical models

Model Term	Modified Models	
	R1 Response	R2 Response
R-sq.	97.04	82.19
R-sq. (adj)	96.23	80.22
R-sq. (pred)	94.55	69.73

However, the coefficient of determination is R-sq. (pred) in the R2 model falls below the acceptable range. The forecasted R-sq. (pred) a score of 53 % suggests that the model possesses a moderate level of predictive capability. This implies that the model possesses a 53 % prediction for future observations based on the independent variables in the model. This low accuracy can be attributed to variables that lack significance, such as the volume of brine, which has $p>0.05$. Variables with $p>0.05$ may have or not have significance on the model [35]. The investigation found that the pH (A) and temperature (B) were significant independent variables affecting the reaction time and percentage of silica extracted, with p-values<0.05. Nevertheless, the second order of the parameters and their products did not have any notable influence. Based on the information obtained from Tables 6 and 7, the models R1 and R2 were modified to eliminate the insignificant terms. Table 7 presents the new R-values. The models' equations for the responses are given in equations 3 and 4.

$$R_1 = 148.03 - 10.750A - 0.3167B + 1.000C \quad (3)$$

$$R_2 = 15.88 + 7.99A + 0.2812B \quad (4)$$

A positive coefficient in Equation 4 indicates that the percentage of silica extraction (R2 response) is directly correlated with the brine pH and temperature. In contrast, the R1 response in Equation 3 exhibits a negative relationship with brine pH and temperature but a positive relationship with brine volume. The relationship between brine pH and the percentage of silica extraction (R2 response) is a positive correlation. This indicates that as the pH level rises, the percentage of silica extraction also increases. Similarly, there is a negative linear relationship between brine pH and the reaction time (R1 response). As the pH level increases, there is a corresponding drop in the reaction time. The phenomenon above is visually illustrated in Figures 8 (a) and (b). The contour lines in Figure 8(b) depict varying reaction times measured in seconds. The hue of the contour lines corresponds to the duration of the reaction time response, with yellow representing shorter durations and green representing longer durations, as specified in the color-coded key located on the right side of the graph.

Figure 9(a) depicts the relationship between the variables (brine pH and brine temperature) and their effects on the percentage of silica extraction. The data suggests that increasing temperatures and certain brine pH levels result in larger extraction rates of silica, indicating a correlation between these factors and the percentage of silica removed. Furthermore, as depicted in Figure 9(b), as the temperature rises at high pH values, the percentage of silica extracted likewise increases. These outcomes are a result of the silica's inert and mildly acidic properties, which are enhanced when treated at a high temperature with NaOH solution.

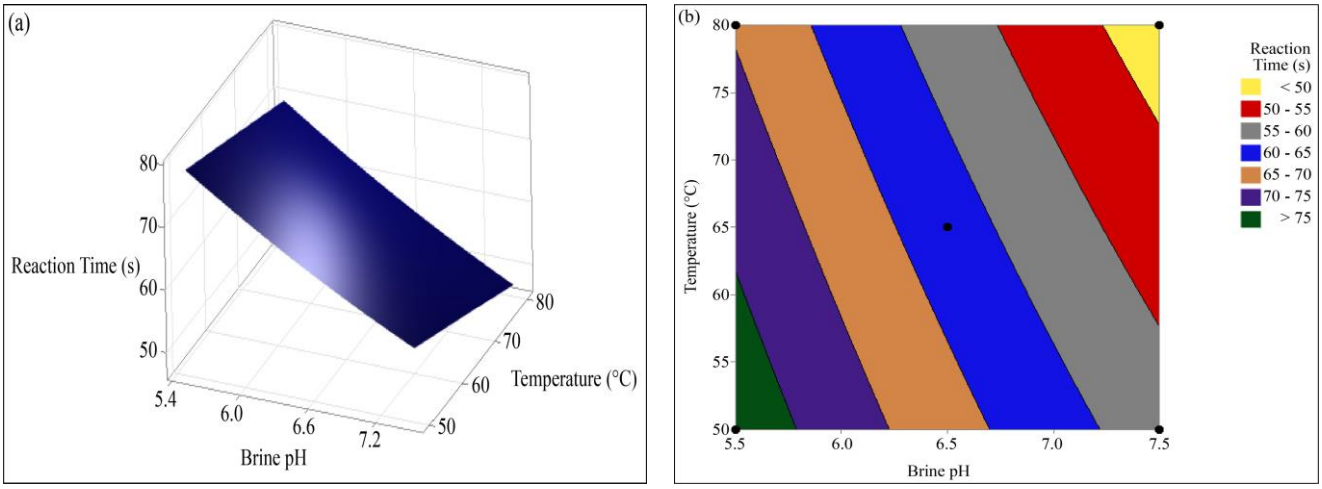

Fig. 8(a) Surface plot, and (b) Contour plot showing how reaction time responded to changes in temperature and pH.

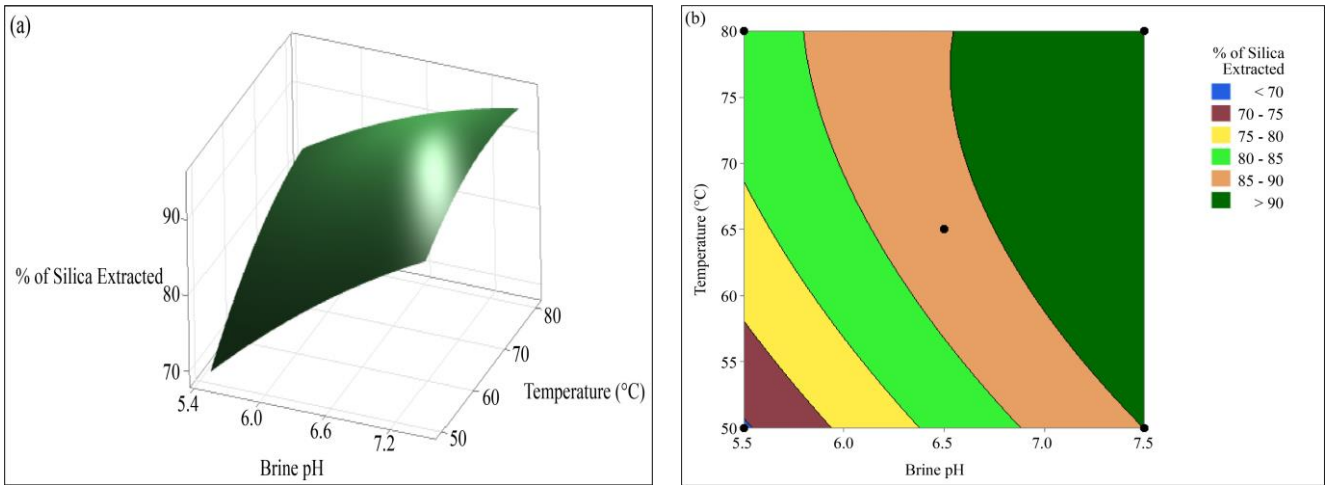

Fig. 9 (a) Surface plot, and (b) Contour plot of % of silica extracted in relation to changes in temperature and pH.

The correlation between the predicted and actual values for the percentage of silica extraction and reaction time responses is shown in Figures 10(a) and (b). PFITS R1 and PFITS R2 refer to the predicted fits, which are predicted values from the regression models. The predicted values from the model were found to be close to the actual experimental values. The percentage error and average percentage error for reaction time were 4.164 % and 0.278 %, respectively. The percentage error and average error for silica extracted were 0.105 % and 0.001 %, respectively. This means that the models accurately captured the behaviour of the model using the Response Surface Model with the training data.

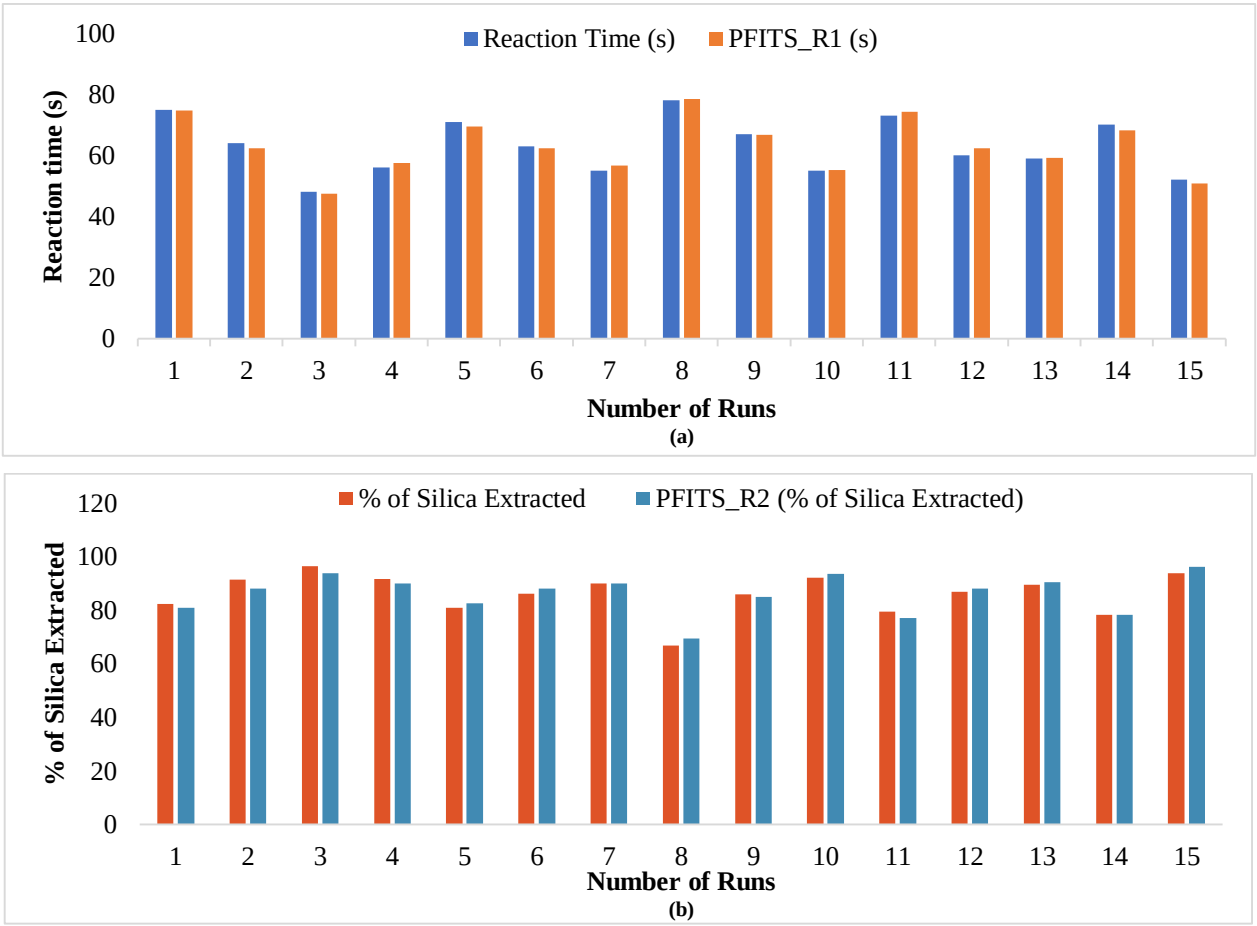

Fig. 10(a) Comparison of predicted reaction time using the empirical model and experimental reaction time, and (b) Comparison of predicted percentage of silica extracted using the empirical model and experimental percentage of silica extracted.

3.2. Residual Plots Analysis

Residual plots are employed in regression and ANOVA tests to assess the quality of the model fit and consequently evaluate the challenges posed by a skewed distribution, outliers, and non-random errors. The Pareto charts in Figures 11 (a) and 12 (a) depict the standardised impacts of three parameters (pH, temperature, volume) on the response variables, namely reaction time and percentage of silica extracted. The pH level has the greatest influence on both the reaction time and the amount of silica extracted. Thus, findings have indicated that pH exerts the most pronounced influence on the formation of silica precipitates in the geothermal brine, followed by temperature. The reference lines located at 1.55 in Figure 11 (a) and at 1.538 in Figure 12 (a) represent the exact value of the t-distribution at a 0.05 level of significance. Factors that have standardized effects greater than 1.55 and 1.538 are deemed to be statistically significant. Figures 11 (b) and 12 (b) demonstrate that the residuals exhibit a normal distribution and typically form a linear pattern, indicating the absence of outliers. When plotted against the fitted values, the residuals indicate a random distribution around zero, suggesting that the residuals possess constant variance and are independent of each other.

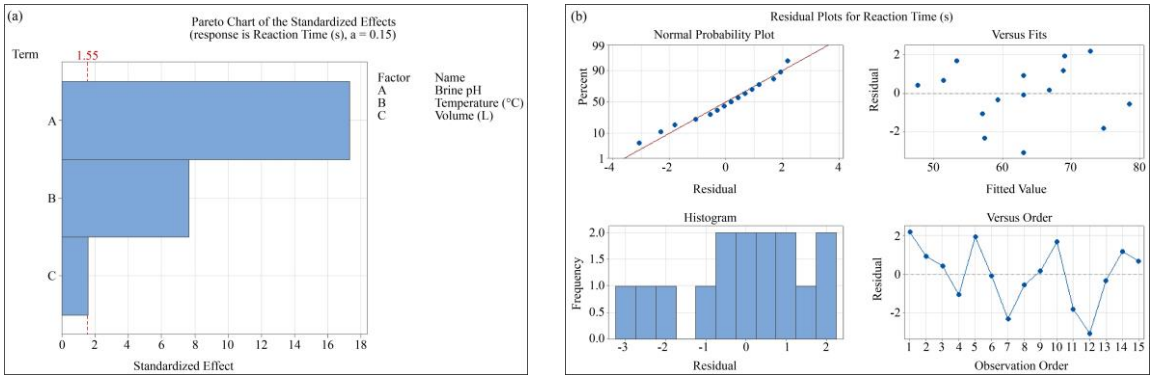

Fig. 11 Model fit analysis for reaction time response using trained data (a) Pareto chart, and (b) Residual plots.

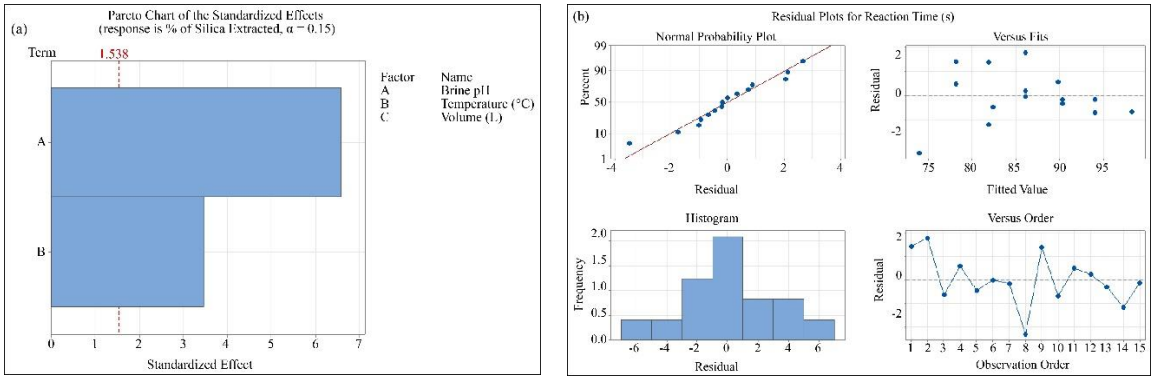

Fig. 12 Model fit analysis for percentage of silica extracted using trained data (a) Pareto chart, and (b) Residual plots.

Both reaction time and silica extracted show statistically significant correlations with pH and temperature. These findings indicate that silica is prone to precipitate under alkaline circumstances, where it reacts with magnesium, forming magnesium silicate. In conclusion, the residual analysis demonstrates that the model adequately fits the data.

3.3. Digital Twin-Augmented Reality Implementation

The AR model was effectively integrated into the physical environment using plane detection, as depicted in Figure 13. The DT-AR model and the APCS were able to work simultaneously in real-time, as shown in Figure 15.

Prior to processing the geofluid in the reactive tank, there were signs of silica scaling building up along the pipeline, causing blockages as the geofluid flowed through, as seen in Figure 16(a). Following the initiation of NaOH dosing, silica precipitation commenced in the reaction tank. The event was the result of a chemical reaction between the dissolved silica and magnesium in the presence of NaOH. As a result, silicate deposits formed at the tank's bottom, as observed in Figure 14, mimicking the reaction that occurred in the APCS's reactive tank.

This strategy effectively handled the issue of pipe blockage, as observed in Figure 16(b). Furthermore, the DT-AR model was able to function independently, mimicking the physical system and capable of evaluating the performance of many parameters prior to their implementation on the actual system as shown in Figure 17.

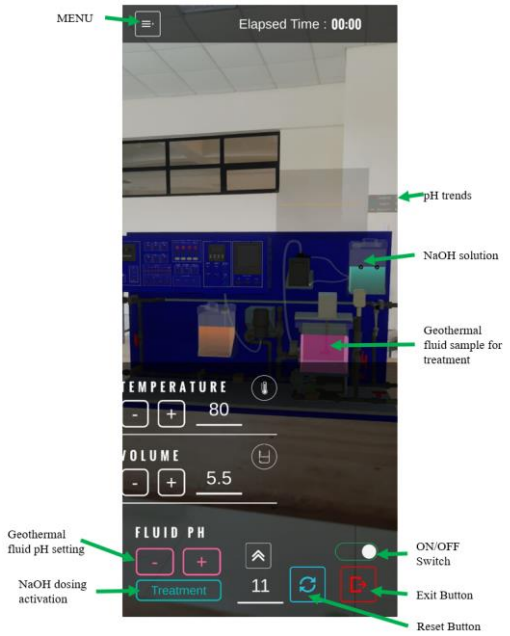

Fig. 13 AR model user interface and virtual model in the physical environment

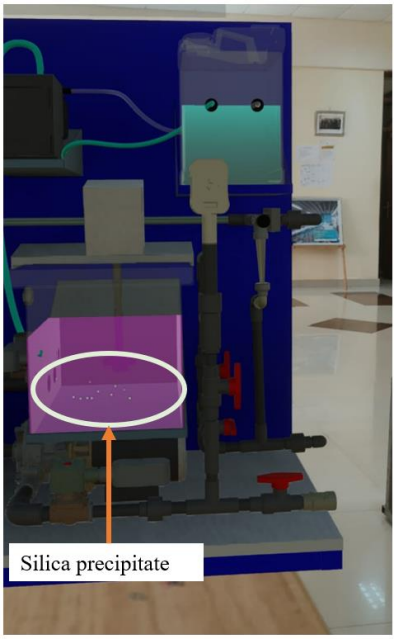

Fig. 14 Silica precipitate observed settling at the bottom of the tank during geofluid treatment

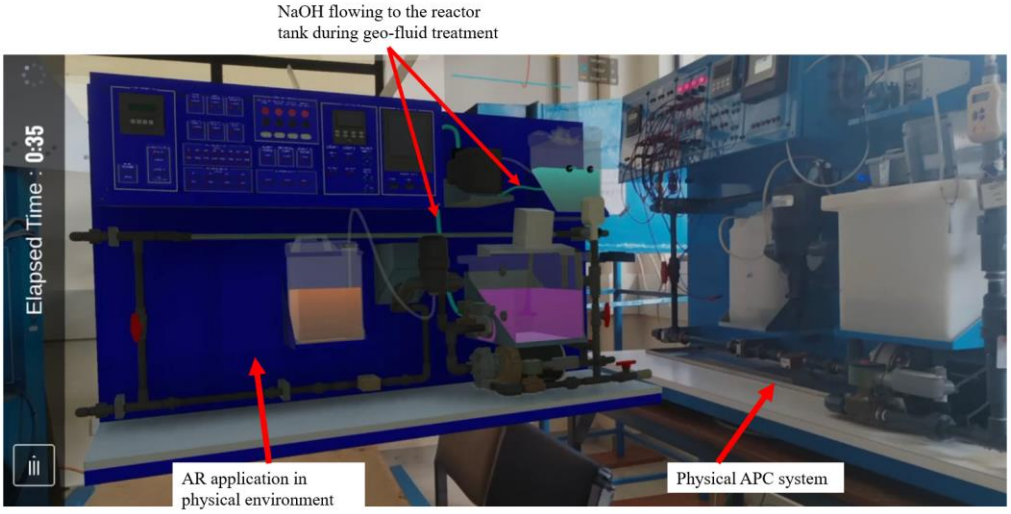

Fig. 15 AR and physical System operating simultaneously

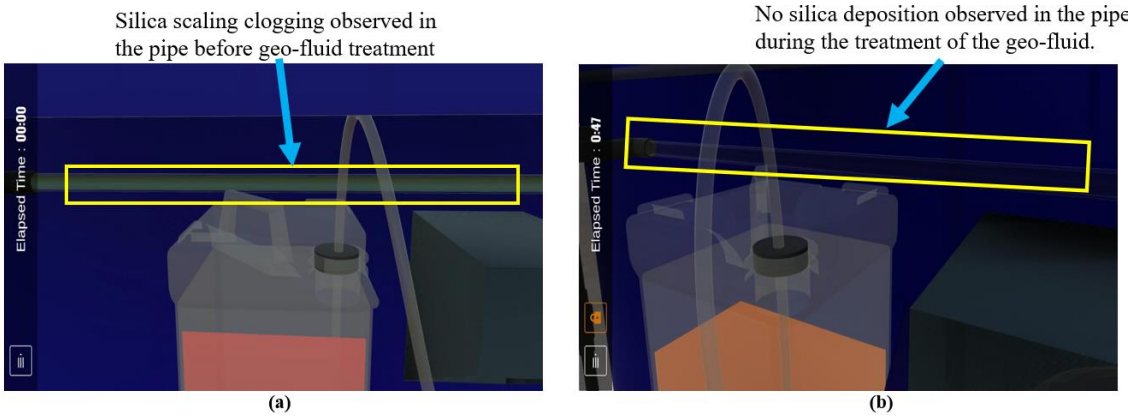

(a) **(b)**

Fig. 16(a) Sections showing silica scaling development in untreated geofluid, and (b) Clear pipe during geofluid treatment.

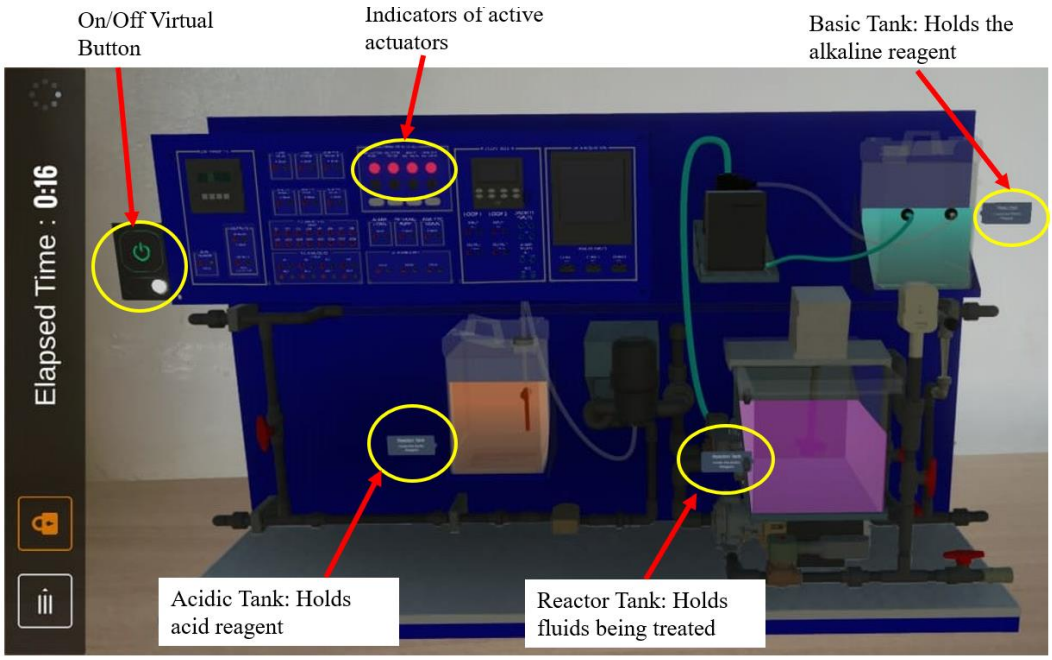

Fig. 17 Standalone DT-AR model

Supervisory control was established through the use of AR, where instructions and commands were transmitted to the physical world for implementation. Real-time communication experiments were conducted to examine events and data handling in both the physical and virtual environments. The virtual environment and mapping interaction enabled the simultaneous execution and activation of activities on the physical equipment, as depicted in Figure 18.

The pH reading from the sensor, pH 8.654626 and other elements were published to a topic (APCS) in the broker and the AR subscribed to the same topic to receive data. Likewise, the setpoint and operational status were published by AR on the same topic and subscribed to by the PLC. Figure 19 shows data published/subscribed to the broker and the pH trends during dosing with NaOH.

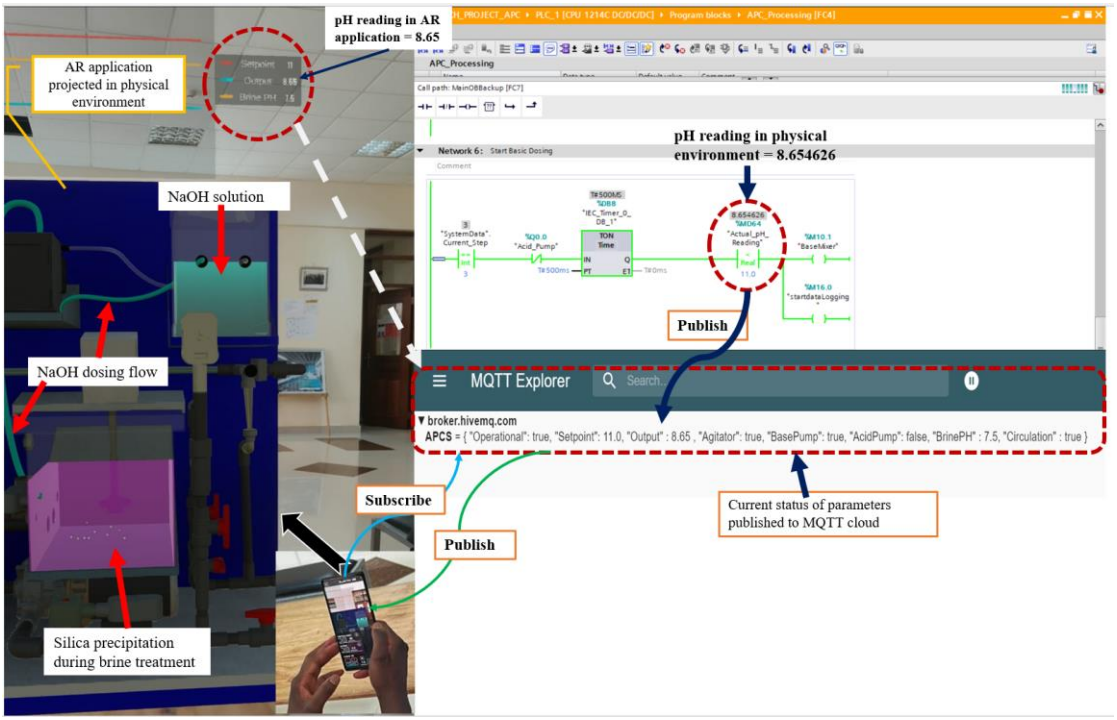

Fig. 18 Physical machine and DT-AR communication via MQTT

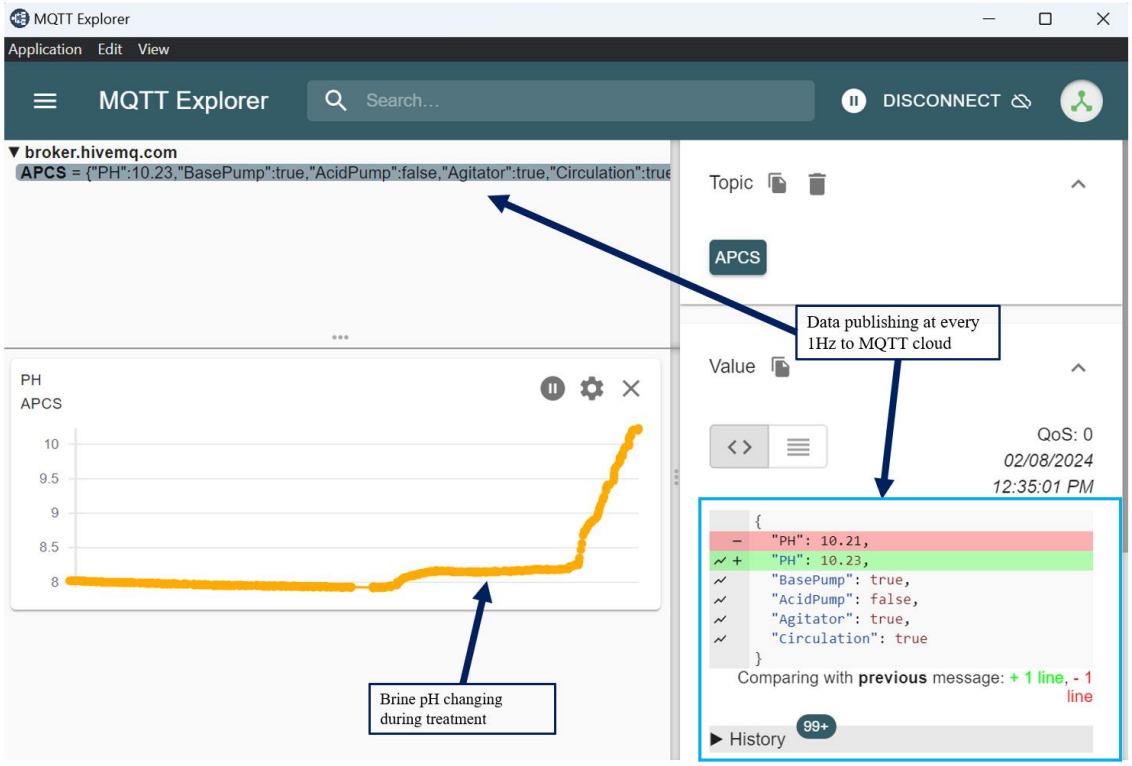

Fig. 19 Data published/subscribed by PLC and AR, respectively, to the broker with the associated topic

The accomplishment of seamless integration between the physical and virtual systems has allowed real-time control of the analytic machine. Because of this, modifying the command signal immediately affected the performance and behaviour of the inputs or outputs.

The DT and AR model accurately replicated the behaviour of geofluids and their reaction to the addition of NaOH solution for pH correction, utilising both historical and real-time data. There was communication between IIoT and the MQTT protocol to establish a seamless connection and enable real-time exchange of data with the APCS. The DT-AR system detected deviations in pH from the SP value and implemented corrective measures by sending a signal to the PLC to modify the dose of NaOH solution. The DT-AR application offered an interactive and immersive experience.

The system offered essential features, information, functionality, and communication capabilities. The system displayed real-time information on the state of the treatment process and the corresponding data from the sensors. In the context of DT, communication was essential. The system provided a bi-directional communication service that allows real-time interaction between physical and virtual elements. Regarding system functionality, it received and executed the commands sent by the operator. It possessed the capability to monitor the advancement of the silica treatment technique.

4. Conclusion

The objective of this study was to regulate the formation of silica deposits in geothermal reinjection wells by utilizing a DT-AR system for real-time monitoring and control. The preliminary experiment specifically analysed the formation of insoluble precipitates in the presence of silicates. The study employed the Response Surface Methodology (RSM) utilising the Box Behnken design to enhance the extraction of silica from geothermal fluid. The optimal parameters for obtaining the maximum silica extraction yield (96.38%) within 48 seconds were a temperature of 80°C, a volume of 5.5 L, and a brine pH of 7.5.

The lowest silica extraction of 66.90 % was observed under the following conditions: pH 5.5, temperature of 50 °C and volume of 5.5. The study determined that the pH of the solution has a substantial impact on the formation of amorphous silica from a geothermal brine when NaOH is introduced.

The significance of temperature in silica extraction in alkaline circumstances is substantial, although volume did not show a major impact. The DT-AR system utilised the MQTT protocol for real-time monitoring and control. Implemented MQTT publish/subscribe architecture for remote sensing and control, integrated IIoT, enabling bidirectional communication between the physical system and AR system.

Acknowledgements

The authors express their gratitude to the Pan African University for providing research funding and to the Siemens Mechatronics Certification Centre at Dedan Kimathi University of Technology (DeKUT) for their cooperation in providing resources for this project.

References

[1] Laveet Kumar et al., "Technological Advancements and Challenges of Geothermal Energy Systems: A Comprehensive Review," *Energies*, vol. 15, no. 23, pp. 1-18, 2022. [CrossRef] [Google Scholar] [Publisher Link]

[2] M.G.J. Shalihin, P. Utami, and M.I. Nurpratama, "The Subsurface Geology and Hydrothermal Alteration of the Dieng Geothermal Field, Central Java: A Progress Report," *IOP Conference Series: Earth and Environmental Science*, vol. 417, pp. 1-12, 2020. [CrossRef] [Google Scholar] [Publisher Link]

[3] Arata Kioka, and Masami Nakagawa, "Theoretical and Experimental Perspectives in Utilizing Nanobubbles as Inhibitors of Corrosion and Scale in Geothermal Power Plant," *Renewable and Sustainable Energy Reviews*, vol. 149, 2021. [CrossRef] [Google Scholar] [Publisher Link]

[4] Argyro Spinthaki et al., "The Precipitation of 'Magnesium Silicate' Under Geothermal Stresses Formation and Characterization," *Geothermics*, vol. 74, pp. 172-180, 2018. [CrossRef] [Google Scholar] [Publisher Link]

[5] Fusun Tut Haklidir, and Mehmet Haklidir, "Fuzzy Control of Calcium Carbonate and Silica Scales in Geothermal Systems," *Geothermics*, vol. 70, pp. 230-238, 2017. [CrossRef] [Google Scholar] [Publisher Link]

[6] Laura Spitzmüller et al., "Selective Silica Removal in Geothermal Fluids: Implications for Applications for Geothermal Power Plant Operation and Mineral Extraction," *Geothermics*, vol. 95, 2021. [CrossRef] [Google Scholar] [Publisher Link]

[7] James H. Johnston et al., "Eliminating the Problematic Deposition of Silica from Separated Geothermal Brine and Enhancing Geothermal Energy Utilisation through a Novel Nanostructured Calcium Silicate Technology: An Overview," *Proceedings World Geothermal Congress*, 2021. [Google Scholar]

[8] Eri Hanajima, and Akira Ueda, "Recovery of Oversaturated Silica from Takigami and Sumikawa Geothermal Brines with Cationic Polymer Flocculants to Prevent Silica Scale Deposition," *Geothermics*, vol. 70, pp. 271-280, 2017. [CrossRef] [Google Scholar] [Publisher Link]

[9] Eko Tri Sumarnadi Agustinus et al., "Scale Prevention Technique to Minimized Scaling on Re-Injection Pipes in Dieng Geothermal Field, Central Java Province, Indonesia," *Indonesian Journal on Geoscience*, vol. 5, no. 2, pp. 129-136, 2018. [CrossRef] [Google Scholar] [Publisher Link]

[10] M. Ridho Ulya et al., "Effect of pH and Surfactant Concentration Sodium Lignosulfonate (SLS) towards Reduction of Silica Mass from Geothermal Brine," *Jurnal Geocelebes*, vol. 7, no. 1, pp. 37-43, 2023. [CrossRef] [Google Scholar] [Publisher Link]

[11] B. Trisakti et al., "Effect of Sulphuric Acid (H_2SO_4) and Sodium Hydroxide (NaOH) Addition to Prevent Silica Scaling in Geothermal Power Plant Projection Pipes at PLTP X," *IOP Conference Series: Materials Science and Engineering*, vol. 801, pp. 1-4, 2020. [CrossRef] [Google Scholar] [Publisher Link]

[12] Tuğba Isık et al., "A Brief Overview on Geothermal Scaling," *Bulletin of the Mineral Research and Exploration*, no. 171, pp. 185-203, 2023. [CrossRef] [Google Scholar] [Publisher Link]

[13] Felix Arie Setiawan et al., "Kinetics of Silica Precipitation in Geothermal Brine with Seeds Addition: Minimizing Silica Scaling in a Cold Re-Injection System," *Geothermal Energy*, vol. 7, no. 1, pp. 1-16, 2019. [CrossRef] [Google Scholar] [Publisher Link]

[14] Argyro Spinthaki et al., "Antiscalant-Driven Inhibition and Stabilization of 'Magnesium Silicate' Under Geothermal Stresses: The Role of Magnesium-Phosphonate Coordination Chemistry," *Energy and Fuels*, vol. 32, no. 11, pp. 11749-11760, 2018. [CrossRef] [Google Scholar] [Publisher Link]

[15] A.D.P Putera et al., "Assessing Silica Precipitation Using Calcium Hydroxide Addition on Dieng's Geothermal Brine," *IOP Conference Series: Earth and Environmental Science*, vol. 200, pp. 1-6, 2018. [CrossRef] [Google Scholar] [Publisher Link]

[16] Asif Matin et al., "Scaling of Reverse Osmosis Membranes Used in Water Desalination: Phenomena, Impact, and Control; Future Directions," *Desalination*, vol. 455, pp. 135-157, 2019. [CrossRef] [Google Scholar] [Publisher Link]

[17] Paolo Taddei Pardelli et al., "Design of a Scaling Reduction System for Geothermal Applications," *E3S Web of Conferences*, vol. 238, pp. 1-10, 2021. [CrossRef] [Google Scholar] [Publisher Link]

[18] E.K. Mroczek, D. Graham, and L. Bacon, "Removal of Arsenic and Silica from Geothermal Fluid by Electrocoagulation," *Journal of Environmental Chemical Engineering*, vol. 7, no. 4, 2019. [CrossRef] [Google Scholar] [Publisher Link]

[19] Yoshihiko Sano, and Masataka Yamaguchi, "Preventing Silica Scale Formation using Hydroxide Ions Generated by Water Electrolysis," *Membranes*, vol. 9, no. 11, pp. 1-17, 2019. [CrossRef] [Google Scholar] [Publisher Link]

[20] Takuya Okazaki et al., "Fiber Optic Sensor for Real-Time Sensing of Silica Scale Formation in Geothermal Water," *Scientific Reports*, vol. 7, no. 1, pp. 1-7, 2017. [CrossRef] [Google Scholar] [Publisher Link]

[21] Fei Tao et al., "Digital Twin-Driven Product Design, Manufacturing and Service with Big Data," *International Journal of Advanced Manufacturing Technology*, vol. 94, no. 9-12, pp. 3563-3576, 2018. [CrossRef] [Google Scholar] [Publisher Link]

[22] Yu Zheng, Sen Yang, and Huanchong Cheng, "An Application Framework of Digital Twin and Its Case Study," *Journal of Ambient Intelligence and Humanized Computing*, vol. 10, no. 3, pp. 1141-1153, 2019. [CrossRef] [Google Scholar] [Publisher Link]

[23] Toqeer Ali Syed et al., "In-Depth Review of Augmented Reality: Tracking Technologies, Development Tools, AR Displays, Collaborative AR, and Security Concerns," *Sensors*, vol. 23, no. 1, pp. 1-54, 2023. [CrossRef] [Google Scholar] [Publisher Link]

[24] Gustavo Caiza, and Ricardo Sanz, "Digital Twin to Control and Monitor an Industrial Cyber-Physical Environment Supported by Augmented Reality," *Applied Sciences*, vol. 13, no. 13, pp. 1-14, 2023. [CrossRef] [Google Scholar] [Publisher Link]

[25] Alexios Papacharalampopoulos, and Panagiotis Stavropoulos, "Towards a Digital Twin for Thermal Processes: Control-Centric Approach," *Procedia CIRP*, vol. 86, pp. 110-115, 2020. [CrossRef] [Google Scholar] [Publisher Link]

[26] Chan Qiu et al., "Digital Assembly Technology Based on Augmented Reality and Digital Twins: A Review," *Virtual Reality and Intelligent Hardware*, vol. 1, no. 6, pp. 597-610, 2019. [CrossRef] [Google Scholar] [Publisher Link]

[27] Syed Mobeen Hasan et al., "Augmented Reality and Digital Twin System for Interaction with Construction Machinery," *Journal of Asian Architecture and Building Engineering*, vol. 21, no. 2, pp. 564-574, 2022. [CrossRef] [Google Scholar] [Publisher Link]

[28] Iraklis Konstantopoulos et al., "Deploying Digital Twins for Geothermal Operations with the GOOML Framework," *Proceedings 48th Workshop on Geothermal Reservoir Engineering*, pp. 1-7, 2023. [Google Scholar] [Publisher Link]

[29] Grant Buster et al., "A New Modeling Framework for Geothermal Operational Optimization with Machine Learning (GOOML)," *Energies*, vol. 14, no. 20, pp. 1- 2021. [CrossRef] [Google Scholar] [Publisher Link]

[30] Nicole Taverna et al., "Data Curation for Machine Learning Applied to Geothermal Power Plant Operational Data for GOOML: Geothermal Operational Optimization with Machine Learning," *Proceedings 47th Workshop on Geothermal Reservoir Engineering*, 2022. [Google Scholar] [Publisher Link]

[31] S.M. Shende et al., Indian Bureau of Mines, Project Credit Formulation & General Guidance Collection and Compilation of Technical Data, 2012.

[32] Yang, Method for the Determination of Silica in Water Application Note. [Online]. Available: http://www.perseena.com

[33] Kristina Wärmefjord et al., "Digital Twin for Variation Management: A General Framework and Identification of Industrial Challenges Related to the Implementation," *Applied Sciences*, vol. 10, no. 10, pp. 1-16, 2020. [CrossRef] [Google Scholar] [Publisher Link]

[34] Usman Ghani et al., "Hydrothermal Extraction of Amorphous Silica from Locally Available Slate," *ACS Omega*, vol. 7, no. 7, pp. 6113-6120, 2022. [CrossRef] [Google Scholar] [Publisher Link]

[35] Murad Alsawalha, "An approach utilizing the Response Surface Methodology (RSM) to optimize Adsorption-Desorption of Natural Saudi Arabian Diatomite- with the Box- Behnken Design Technique," *Arabian Journal of Chemistry*, vol. 16, no. 1, pp. 1-12, 2023. [CrossRef] [Google Scholar] [Publisher Link]